Original Article

Toxicologic Pathology
2018, Vol. 46(1) 62-74

DOI: 10.1177/0192623317732303
journals.sagepub.com/home/tpx
SAGE

Length, but Not Reactive Edges, of Cup-stack MWCNT Is Responsible for Toxicity and Acute Lung Inflammation

Raymond F. Hamilton Jr.[1], Shuji Tsuruoka[2], Nianqiang Wu[3], Michael Wolfarth[4], Dale W Porter[4], Melisa Bunderson-Schelvan[1], and Andrij Holian[1]

Abstract

Multiwalled carbon nanotube (MWCNT) toxicity after inhalation has been associated with size, aspect ratio, rigidity, surface modification, and reactive oxygen species production. In this study, we investigated a series of cup-stacked MWCNT prepared as variants of the Creos 24PS. Mechanical chopping produced a short version (AR10) and graphitization to remove active reaction sites by extreme heat (2,800°C; Creos 24HT) to test the contribution of length and alteration of potential reaction sites to toxicity. The 3 MWCNT variants were tested *in vitro* in a human macrophage–like cell model and with C57BL/6 alveolar macrophages for dose-dependent toxicity and NLRP3 inflammasome activation. The 24PS and 24HT variants showed significant dose-dependent toxicity and inflammasome activation. In contrast, the AR10 variant showed no toxicity or bioactivity at any concentration tested. The *in vivo* results reflected those observed *in vitro*, with the 24PS and 24HT variants resulting in acute inflammation, including elevated polymorphonuclear counts, Interleukin (IL)-18, cathepsin B, and lactate dehydrogenase in isolated lung lavage fluid from mice exposed to 40 μg MWCNT. Taken together, these data indicate that length, but not the absence of proposed reaction sites, on the MWCNT influences particle bioactivity.

Keywords

MWCNT, macrophage, NLRP3 inflammasome, ROS, nanomaterials

Engineered carbon nanomaterials such as multiwalled carbon nanotubes (MWCNTs) have applications in structural and electronic devices, attributable to their extraordinary thermal conductivity, mechanical, and electrical properties, creating a potential occupational exposure situation (Donaldson et al. 2006). The potential bioactivity (*in vitro* toxicity and increased production of inflammatory mediators and/or increased inflammation and pathology *in vivo*) of MWCNT has been attributed to length (Murphy et al. 2011; Palomaki et al. 2011; Hamilton, Wu, et al. 2013), diameter/thickness (Fenoglio et al. 2012), aggregation state (Qu et al. 2009; Wang et al. 2011), metal contaminants (Hamilton et al. 2012; Hamilton, Girtsman, et al. 2013; Liu et al. 2008), aspect ratio/rigidity (Palomaki et al. 2011; Donaldson et al. 2010), and release of reactive oxygen species (ROS; Nel et al. 2006; Palomaki et al. 2011). Considering the potential variables (listed above) available in MWCNT and that MWCNT can be assembled by numerous differential procedures, more data are necessary to fully understand what MWCNT properties contribute to toxicity. Due to the method of generation, cup-stack MWCNTs have not received as much attention as MWCNT prepared by other procedures. Cup-stack MWCNTs present many terminal ends that may contribute to unique biological activity (Tsuruoka, Matsumoto, Koyama, et al. 2015; Lehman et al. 2011). Thus, cup-stack MWCNT variants were examined in this study *in vitro* and *in vivo*.

MWCNT may have distinct biological effects when inhaled (D. W. Porter et al. 2010; D. W. Porter et al. 2012; Murphy et al. 2011). Several studies have focused on particle retention in the lung, linked to MWCNT length or rigidity, as a potential area of concern (Murphy et al. 2011; Mercer et al. 2010;

[1] Department of Biomedical and Pharmaceutical Sciences, Center for Environmental Health Sciences, University of Montana, Missoula, Montana, USA
[2] Institute of Carbon Science and Technology, Shinshu University, Nagano, Japan
[3] Department of Mechanical and Aerospace Engineering, West Virginia University, Morgantown, West Virginia, USA
[4] National Institute for Occupational Safety and Health, Morgantown, West Virginia, USA

Corresponding Author:
Andrij Holian, Department of Biomedical and Pharmaceutical Sciences, Center for Environmental Health Sciences, University of Montana, 32 Campus Drive—280 Skaggs, Missoula, MT 59812, USA.
Email: andrij.holian@umontana.edu

Donaldson et al. 2010). Still other studies cite MWCNT diameter as the particle property that affects *in vivo* bioactivity (Fenoglio et al. 2012; Hamilton, Wu, et al. 2013). Nevertheless, it is apparent that MWCNT size (length and/or diameter) is a critical factor in MWCNT-induced lung pathology.

For nanomaterial interactions at the cellular level, a number of studies have linked phago-lysosomal membrane permeabilization (LMP) accompanied by cathepsin B release, initiating NLRP3 (Nucleotide-binding oligomerization domain [NOD]-like receptor pyrin domain containing 3) inflammasome assembly, and, in turn, caspase-1 activation as critical steps in nanoparticulate-induced inflammation (Tschopp and Schroder 2010; Martinon, Mayor, and Tschopp 2009; Arend, Palmer, and Gabay 2008; Hamilton et al. 2009: Hamilton et al. 2012). This sequence of events has been confirmed using MWCNT in more recent studies (Hamilton, Xiang, et al. 2013; Hamilton, Wu, et al. 2013). Particle-induced ROS production has also been linked to NLRP3 inflammasome activation by various studies (Dostert et al. 2008; Palomaki et al. 2011; Tschopp and Schroder 2010). However, it is not clear whether cytosolic ROS directly cause NLRP3 inflammasome activation (Tschopp and Schroder 2010) or are a result of LMP, contributing to mitochondrial damage (M. Yang et al. 2014). While there is evidence that ROS are involved in particle-induced acute inflammation, the exact causal sequence remains to be resolved. Furthermore, the mechanisms by which particles induce LMP as well as the contribution of ROS to that process are also unclear (M. Yang et al. 2014).

In this study, we used cup-stack MWCNT to test the hypothesis that MWCNT length is a more important determinant for particle-induced bioactivity, both *in vitro* and *in vivo*, than that of potential reactive centers on surfaces after particle exposure. A long cup-stack MWCNT variant (24PS) was graphitized by extreme heat (24HT); alternatively, 24PS was mechanically chopped to form a short variant of the original (AR10). *In vitro* assessments of MWCNT bioactivity were conducted using primary alveolar macrophages (AM) isolated from C57Bl/6 mice and differentiated human THP-1 cells with respect to toxicity and NLRP3 inflammasome activation. *In vivo* studies involved C57BL/6 mice instilled with the same MWCNT particles that were examined 1 day after instillation to determine inflammation and release of inflammatory mediators in the lung.

Materials and Methods

MWCNT Heat Treatment

MWCNT high-temperature annealing was carried out in a graphite-resistance furnace operating in a high-purity argon gas atmosphere as previously described; the AR10 material was also previously described (Tsuruoka, Matsumoto, Castranova, et al. 2015; Tsuruoka, Matsumoto, Koyama, et al. 2015). The heating rate increase was 20°C per min and the target temperature of 2,800°C was maintained for 30 min. Then, the furnace was cooled down to room temperature (average laboratory temperature) in the argon gas atmosphere. Residual iron and sulfur content were measured by X-ray fluorescence analysis (Rigaku ZSX mini) with a Pd K_α X-ray source. The measurable limit was 30 ppm for iron and 100 ppm for sulfur. A JEOL X-ray diffractometer system (JDX-3532) was used to characterize the composition of carbon nanotube impurities with a Cu K_α X-ray source. To compare the absolute X-ray diffraction intensity of different samples, a 40-mg sample was fixed in a 25 mm × 20 mm × 1.5 mm sample holder (Menendez et al. 1996). Transmission electron microscopy images of the source 24PS MWCNT and the 24HT MWCNT with loop structure can be found in Figure 1.

MWCNT Characterization

Particle size and zeta potential were measured in culture media at 25°C using a Malvern Zetasizer Nano Zen 3600 (Malvern Instruments, Worcestershire, UK) at a 90° detector angle. Endotoxin contamination was determined by washing/sonicating 1 mg/ml carbon nanotubes (CNT) in endotoxin-free water for 30 min followed by centrifugation at 16,000 ×g for 15 min prior to assay. The assay (ToxinSensor) was performed on isolated supernatant according to the manufacturer's protocol (GenScript, Piscataway, NJ). Aggregate size was expressed as nm ± the standard deviation. Zeta potentials are expressed as mV ± standard deviation. Endotoxin contamination is expressed as ng endotoxin/5 μg CNT, which represents the largest mass of CNT added to the cells (50 μg/ml). Results are found in Table 1.

MWCNT Suspensions

All MWCNT were weighed and suspended in either sterile 7.5% bovine serum albumin/phosphate buffered saline (BSA/PBS; Sigma, St Louis, MO) or dispersion media (DM), depending on whether the experiment was *in vitro* or *in vivo*. DM was used for all *in vivo* particle instillations; the exact formulation can be found elsewhere (D. Porter et al. 2008). Particle suspensions were sonicated for 2 min at half-max power in a Masonix cup-horn sonicator (XL2020, Farmingdale, NY) attached to a Forma circulating water bath at 550 W and 20 Hz (8,000 J) at a stock concentration of 5 mg/ml for *in vitro* experiments and varying concentrations for *in vivo* instillations.

In Vitro *Experimental Procedures*

AM isolation and cell culture

Animals. C57Bl/6 (2-months old, male) were housed in controlled environmental conditions (22 ± 2°C; 30–40% humidity, 12-hr light:12-hr dark cycle) and provided food and water *ad libitum*. All procedures were performed under protocols approved by the Institutional Animal Care and Use Committee of the University of Montana.

AM isolation. Mice were euthanized by sodium pentobarbital (Euthasol™ Schering-Plough, lot# 1JRR11V), and the lungs with the heart were removed. Lung lavage was performed using ice-cold PBS (pH 7.4). Lung lavage cells were isolated by centrifugation (400 ×*g*, 5 min, 4°C) and cell counts obtained using a Coulter Z2 particle counter (Beckman Coulter, Miami, FL).

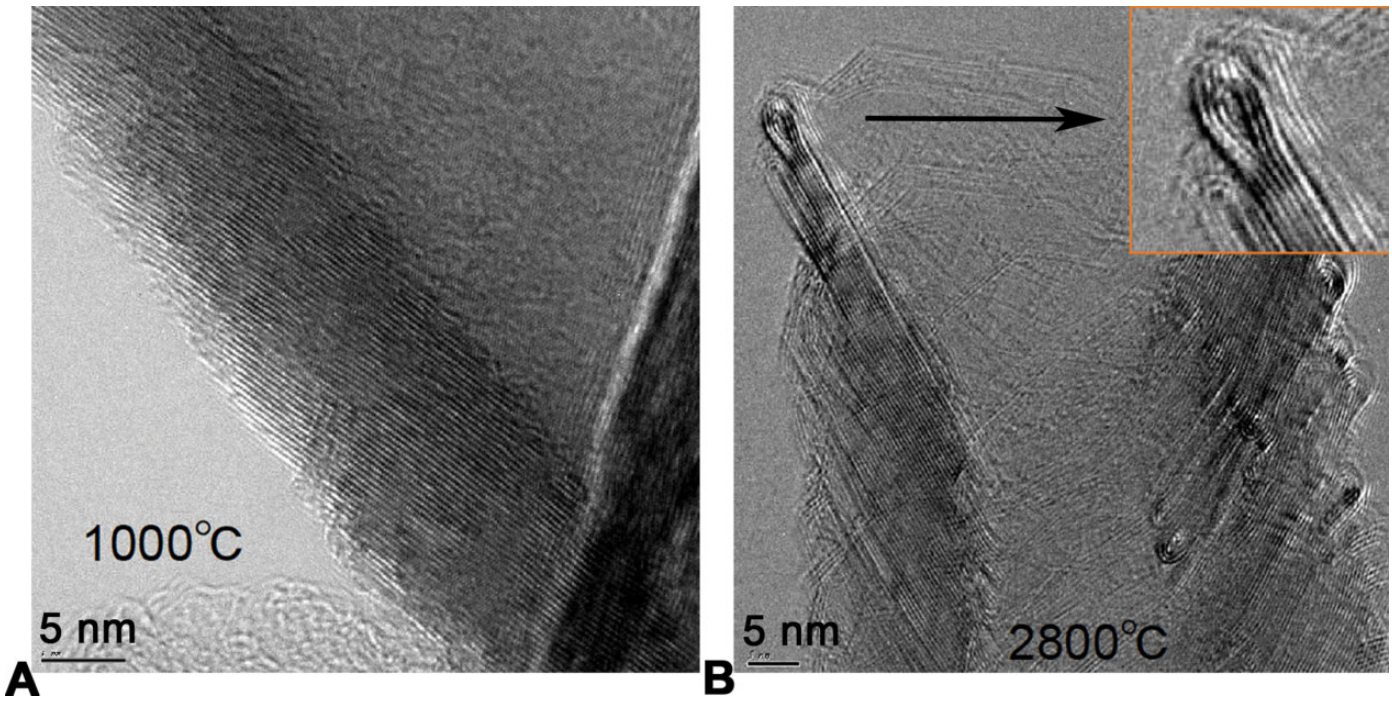

Figure 1. Transmission electron microscopy image showing development of the loop structures on the 24PS multiwalled carbon nanotubes (MWCNTs) at high temperature: (A) Source 24PS MWCNT and (B) 24HT MWCNT at 2,800°C. Inset: high magnification of the loop structure.

Table 1. Complete Characterization of GSI CREOS MWCNT.

		MWCNT		
Property	Method of Determination	24PS	24HT	AR10
Outer diameter (nm) mean	SEM, TEM	70–80	70–80	70–80
Outer diameter (nm) distribution	SEM, TEM	40–120	40–120	40–120
Inner diameter (nm) distribution	TEM	30–70	30–70	30–70
Mean length (μm)	SEM	5	5	1
Aspect ratio (L/D)		70	70	14
d_{002}	XRD	0.3424	0.3378	nd
Real density (g/cm^3)	Helium substitution	2.073	nd	nd
Bulk density (g/cm^3)	JIS K6720-2	0.07	0.07	0.26
Specific surface area (m^2/g)	N_2-BET	50	50	70
Starting temperature of oxidation (°C)	TG/DTA	520	770	520
Electrical resistance in bulk state (Ω·cm)	4-Pin probe	0.033	0.007	0.045
Moisture content	Weight loss	<1.0%	<0.5%	<1.0%
Ash content	Weight loss	<2.0%	0	<2.0%
Iron content	AAS	<1.4%	<100 ppm	<1.4%
Surface hydrocarbon content	Soxhlet extraction	<0.1%	0	<0.1%
Aggregate size (nm) in RPMI media (mean ± *SD*)	DLS	377.3 ± 39.31	384.7 ± 117.2	274.3 ± 14.19
Aggregate size (nm) in dispersion media (mean ± *SD*)	DLS	397.3 ± 39.93	431 ± 117.2	262 ± 13.08
Zeta potential (mV) in RPMI media (mean ± *SD*)	DLS	11.17 ± 0.115	10.63 ± 0.29	11.15 ± 1.21
Zeta potential (mV) in dispersion media (mean ± *SD*)	DLS	11.5 ± 0.66	11.83 ± 1.2	12.1 ± 0.94

Note: Highlighted section shows the data relevant to reactive oxygen species potential of the MWCNT variants. MWCNT = multiwalled carbon nanotube; *SD* = standard deviation; TEM = transmission electron microscopy; SEM = standard error of the mean; XRD = X-ray diffraction; DLS = dynamic light scattering; TG/DTA = thermogravimetry and differential thermal analysis; N2-BET = nitrogen Brunauer-Emmett-Teller; JIS = Japanese Industrial Standard; AAS = atomic absorption spectroscopy; nd = not determined.

Cell culture. AMs were suspended in RPMI media supplemented with 10% fetal bovine serum, 0.05 mM 2-mercaptoethanol, sodium pyruvate, and supplemented with an antimycotic/antibiotic cocktail (Mediatech, Manassas, VA). Cells were suspended at 1×10^6 cells per ml and then lipopolysaccharide (LPS, Sigma, St Louis, MO) at 20 ng/ml was added to stimulate pro-IL-1β formation. A 100 μl sample (1×10^5 cells) of cells was exposed to each MWCNT

(eg: high-dose 50 μg/ml equivalent to 5 μg/10^5 cells equivalent to 15.62 μg/cm^2 [5 μg on 0.32 cm^2]); experiments were conducted in 96-well plates for 24 hr in 37°C water-jacketed CO_2 incubators (ThermoForma, Houston, TX). Particle concentrations included 0, 10, 25, and 50 μg/ml. Media was collected for the IL-1β assay, and cell viability was determined by 3-(4,5-dimethylthiazol-2-yl)-5-(3-carboxymethoxyphenyl)-2-(4-sulfophenyl)-2H-tetrazolium (MTS) assay and lactate dehydrogenase (LDH) release. Ten to 12 mouse lung lavage collections were pooled, and this experiment was replicated 3 times.

Human THP-1 cell line culturing. Previously, this model was fully characterized as a nanoparticle screening tool (Xia et al. 2013). THP-1 cells, a human monocytic cell line obtained from American Type Culture Collection (ATCC), were suspended in RPMI media (MediaTech, Manassas, VA) supplemented with 10% fetal bovine serum, 50 μM beta-mercaptoethanol, 1 mM sodium pyruvate, 250 ng/ml amphotericin B, and 100 U/ml penicillin and streptomycin (all supplements Media Tech, Manassas, VA) in 75 cm^2 flasks at 37°C. The cells in suspension were differentiated into a macrophage-like cell by adding 150 nM Vitamin D_3 (1α, 25-dihydroxy, EMD Millipore, Darmstadt, Germany) for 24 hr. The resulting semiadherent cells were scraped with a rubber policeman in the existing media (Corning, Corning, NY). The loose cells were then centrifuged at 400 ×*g* for 5 min, the resulting cell pellet was resuspended in 1 ml complete media; a 40 μl sample was then counted on a Z2 Coulter Counter (Beckman Coulter, Miami, FL). The cells were suspended at 1×10^6 cells/ml and a small amount of phorbol 12-myristate 13-acetate (5 nM PMA [phorbol 12-myristate 13-acetate], Sigma) and LPS (10 ng/ml LPS, Sigma) was added. PMA costimulation is necessary to stimulate aggressive phagocytosis of the MWCNT. LPS costimulation is necessary to induce NF-κB translocation, leading to pro-IL-1β synthesis and NLRP3 inflammasome-induced IL-1β release in the transformed THP-1 model (Palomaki et al. 2011; Dostert et al. 2008). Cells (350 μl) were then pipetted into 1.5 ml microfuge tubes. The MWCNT conditions were added (from 5 mg/ml concentrated stock suspensions) to the cells at a final concentration of 25 μg/ml. The MWCNT variants were used at a range of concentrations (0, 6.25, 12.5, 25, and 50 μg/ml). The resulting cell/particle suspension was mixed by pipette action. The cells were then transferred to 96-well tissue culture plates at 100 μl per well in triplicate (1×10^5 cells/well), and cultured for an additional 24 hr. All cultures were maintained in 37°C water-jacketed CO_2 incubators (ThermoForma, Houston, TX). Viability and IL-1β levels were determined as described below. Three experimental replicates were done for each experiment.

Human AM Isolation and Culture

The following procedures were approved by the St. Patrick Hospital/Community Medical Center Joint Investigational Review Board for the protection of human subjects. The lone subject used in this study signed "informed consent" documents.

Isolation of lung cells from human subject. Specific lung lobes were lavaged with instillations of 80 ml sterile saline, which yielded approximately 50 ml lavage fluid per lobe. This was kept on ice until the cell isolation. One to 4 lung lobes were lavaged depending on accessibility and the subject's tolerance for the procedure. Cells were isolated from the lavage fluid by centrifugation at 400 ×*g* (Thermo Forma centrifuge, Marietta, OH). The saline supernatant was aspirated and frozen at −80°C, and the cell pellet was resuspended in a small volume (1–5 ml) of RPMI (Gibco BRL, San Francisco, CA) with 10% heat inactivated, human AB serum (Sigma Chemical, St Louis, MO) with antibiotics (50 U/ml penicillin, 50 μg/ml gentamicin, and 50 μg/ml streptomycin). Cell count was determined with the ZBI Coulter Counter (Beckman Coulter). Broncho alveolar lavage yielded variable cell counts depending on lobe inflammation. Cell differentials were performed by cytocentrifugation (Cytospin 3 Shandon) of 3×10^4 cells and staining with Geimsa staining on a Bayer automated slide stainer (Bayer). Cells were >90% viable by trypan blue exclusion. Cells at 1×10^6/ml were cultured with and without 20 ng/ml LPS for 24 hr in 96-well plates with 50 μg/ml MWCNT as described above at 37°C in a water-jacketed, 5% CO_2 incubator (Thermo Forma, Houston, TX). At the termination of the experiment, culture cells were monitored for viability by MTS assay, and the supernatant was retrieved and frozen at −20°C for later IL-1β assays.

Toxicity Assays

MTS assay. Cell viability/proliferation was determined by MTS using the CellTiter^{96} assay (Promega, Madison, WI) according to the manufacturer's protocol with a modification as described below. This assay uses a colored dye that is read by a colorimetric plate reader (Molecular Devices, Sunnyvale, CA). To avoid artifacts in the optical density values, steps were taken to remove the MTS reagent (transferring it into another plate) from the cell/particle mixture adhered to the plate bottom. The formation of bubbles was avoided and the plate was read at 490 nm.

LDH Assay

Cell viability was confirmed by measuring the release of LDH using the CytoTox^{96} assay (Promega, Madison, WI) according to the manufacturer's protocol. This assay uses 50 μl culture supernatant mixed with the assay substrate for a 10-min reaction and is then stopped with an acidic reagent. The formation of bubbles was avoided, and the plate was read at 490 nm. A positive control was created by lysing an unstimulated control culture 30 min before the assay was conducted, thus releasing 100% of the possible LDH and creating the highest possible value for comparisons. Three experimental replications were performed for all toxicity assays.

Cytokine Assays

Mouse and human IL-1β DuoSets were obtained from R&D Systems (Minneapolis, MN) and ELISA was performed

according to the manufacturer's protocol. IL-18 antibodies (capture and detection) for ELISA were also obtained from R&D Systems. High mobility group box 1 ELISA Plates were read at 450 nm and data expressed as pg/ml in a similar manner to that previously described (Jessop and Holian 2014).

In Vivo *Experimental Procedures*

Animals. Male C57BL/6J mice (6 weeks old) were obtained from Jackson Laboratories (Bar Harbor, ME). Mice were housed 1 per cage in polycarbonate isolator ventilated cages and provided HEPA-filtered air, with fluorescent lighting from 0700 to 1900 hr. Autoclaved Alpha-Dri virgin cellulose chips and hardwood beta-chips were used as bedding. Mice were monitored to be free of endogenous viral pathogens, parasites, mycoplasmas, *Helicobacter* and cilia-associated respiratory *Bacillus*. Mice were maintained on Harlan Teklad Rodent Diet 7913 (Indianapolis, IN), and tap water was provided *ad libitum*. Animals were acclimated for at least 5 days before use. All animals used in this study were housed at the National Institute for Occupational Safety and Health (NIOSH; Morgantown, WV), which is an AAALAC-accredited, specific pathogen-free, environmentally controlled facility. All procedures involving animals were approved by the NIOSH Institutional Animal Care and Use Committee.

Pharyngeal aspiration exposure of mice. MWCNT suspensions were prepared in DM as described above. Mice were anesthetized with isoflurane (Abbott Laboratories, North Chicago, IL) and, when fully anesthetized, the mouse was positioned with its back against a slant board and suspended by the incisor teeth using a rubber band. The mouth was opened and the tongue gently pulled aside from the oral cavity. A 50 µl aliquot of the MWCNT suspension was pipetted at the base of the tongue, and the tongue was restrained until at least 2 deep breaths were completed (but for no longer than 15 s). Following release of the tongue, the mouse was gently lifted off the board, placed on its left side, and monitored for recovery from anesthesia. Mice received a single dose of DM (vehicle control), 2.5, 10, or 40 µg/mouse MWCNT.

Lung lavage. At 24-hr postexposure, mice were euthanized with an intraperitoneal injection of sodium pentobarbital (>100 mg/kg body weight) followed by exsanguination. A tracheal cannula was inserted, and lung lavage was performed through the cannula using ice-cold Ca^{2+} and Mg^{2+}-free PBS (pH 7.4) supplemented with 5.5 mM D-glucose. The first lavage (0.6 ml) was kept separate from the rest of the lavage fluid. Subsequent lavages, each with 1 ml PBS, were performed until 4 ml lavage fluid (in total) was collected. Cells from the lung lavage were isolated by centrifugation (650 $\times g$, 5 min, 4°C). An aliquot of the acellular supernatant from the first lung fluid was decanted and transferred to tubes for analysis of LDH. The acellular supernatants from the remaining lavage samples were decanted and discarded. Cells isolated from the first and subsequent lavages for the same mouse were pooled after resuspension in PBS, centrifuged a second time (650 $\times g$, 5 min, 4°C), and the supernatant decanted and discarded. The cell pellet was then resuspended in PBS and placed on ice. Total cell counts were obtained using a Coulter Multisizer 3 (Coulter Electronics, Hialeah, FL), and cytospin preparations of the cells were made using a cytocentrifuge (Shandon Elliot Cytocentrifuge, London). The cytospin preparations were stained with modified Wright-Giemsa stain, and cell differentials were determined by light microscopy.

Lung lavage fluid LDH activity measurements. LDH activities were evaluated as a marker of cytotoxicity. LDH activities were determined by monitoring the LDH-catalyzed oxidation of lactate to pyruvate coupled with the reduction in NAD^+ (Nicotinamide adenine dinucleotide$^+$)at 340 nm using a commercial assay kit (Roche Diagnostics Systems, Montclair, NJ) and COBAS MIRA Plus instrument (Roche Diagnostic Systems, Montclair, NJ).

Lung lavage fluid cathepsin activity. As previously described by our laboratory (Sager et al. 2014), B-specific cathepsin activities were determined by mixing the following assay components in a 96-well plate using PBS as the diluent: lavage fluid (50 µl) and 2 µg Z-LR-AMC (fluorogenic Peptide Substrate, R&D Systems, Minneapolis, MN) $\pm$ 66 µM inhibitor (Z-Phe-Phe-FMK, MBL International, Woburn, MA) in a total volume of 150 µl. The assay samples were incubated at 37°C for 1 hr, fluorescence was then measured using a plate reader at 380 nm excitation and 460 nm emission. Cathepsin B-specific activity was calculated as follows: relative fluorescent units from assay without inhibitor minus the assay with inhibitor.

Confocal imaging of C57BL/6 AM exposed to MWCNT. Mouse AMs were collected as described earlier. The cells were distributed in culture media at 10^6/ml. The cell suspension and particles were mixed briefly in an Eppendorf tube, and 300 µl of cell/particle mixture was pipetted in to a single chamber of an 8-chamber Lab-Tek Chambered Coverglass (Thermo). This chambered cover glass was incubated for 24 hr in a 37°C water-jacketed CO_2 incubator. At the end of the incubation, the chambers were aspirated to remove the media and washed once in PBS. This was removed and replaced with PBS containing a green membrane stain $DiOC_{18}(3)$ and a nucleic acid counterstain propidium iodide immediately prior to imaging. Stains were diluted at 1,000× as supplied in the LIVE/DEAD cell-mediated cytotoxicity kit (L7010) from Molecular Probes (Eugene, OR). The PBS/stain solutions were aspirated and replaced with PBS after 30-min incubator exposure. Green cells indicated living cells. Red nuclei indicated dead cells. The yellow staining of the MWCNT resulted from the carbon particles absorbing the stains equally. Imaging was done on an Olympus Fluoview FV1000 MPE 1x81 Laser Scanning Biological Microscope and FV10-ASW, v4.2a software. The 40× Uapo objective in oil immersion (NA 1.35) was used. The 488 and 559 laser lines were used for excitation. $DiOC_{18}(3)$ had an excitation and emission spectra of 484 nm and 501 nm,

respectively. Propidium iodide had an excitation and emission spectra of 536 nm and 617 nm, respectively. The confocal aperture was 110 μm. Images were collected at 1024 × 1024 box size with 2.58 μm/pixel.

Statistical Analyses

Statistical analyses involved comparison of means using a 1- or 2-way analysis of variance followed by Dunnett's test or Sidak's adjustment to compensate for increased type I error resulting from pairwise mean comparisons. All probabilities were 2-tailed unless otherwise stated. Statistical power was greater than 0.8. Statistical significance was defined as a probability of type I error occurring at less than 5% ($p < .05$). The minimum number of experimental replications was 3. Graphics and analyses were performed on PRISM 7.0.

Results

Particles

All 3 MWCNT were provided by GSI Creos Corp (Tokyo, Japan) as previously described. The 24PS original MWCNT was synthesized using a cup-stack carbon nanotube process and determined to be 5 μm long and 75 nm wide. The process used to create the 24HT MWCNT was described above to effectively remove the cup-stack edges while retaining the aspect ratio of the original material. Upon heating, the edge sites of the graphitic bond released hydrogen. When hydrogen gas is released over 1,000°C, the edge sites must be energetically stabilized through loop morphology between adjacent active end planes on the inner and outer surfaces of the MWCNT. This reformation or loop structure can be clearly observed above 1,800°C (Figure 1B). The AR10 MWCNT was created by mechanically chopping the original 24PS in a proprietary process, thus creating a 1-μm version of the original 24PS and retaining all of the cup-stack edges of the original material. A comprehensive list of physical characterizations for all 3 MWCNT can be found in Table 1. The 2 modifications of the original MWCNT allowed for direct testing of the hypothesis that length is a more critical factor than the presence of reactive edges regarding MWCNT-induced toxicity and NLRP3 inflammasome activation.

THP-1 Cytotoxicity and NLRP3 Inflammasome Activation

The 3 MWCNT variants were first tested in a THP-1 human cell line optimized for particle interactions as described in Methods section. Figure 2A and 2B shows the toxicity of these nanomaterials in a 24-hr culture at various concentrations ranging from 6.25 μg/ml to 50 μg/ml. The LDH assay in Figure 2A shows that both the original cup-stack 24PS and the heated 24HT MWCNT at the highest concentration tested produced significantly higher levels of toxicity (though still relatively low) than those of the 0 μg/ml control and the AR10 chopped MWCNT at the same concentration (50 μg/ml). In contrast, the MTS assay in Figure 2B demonstrates that only the heated

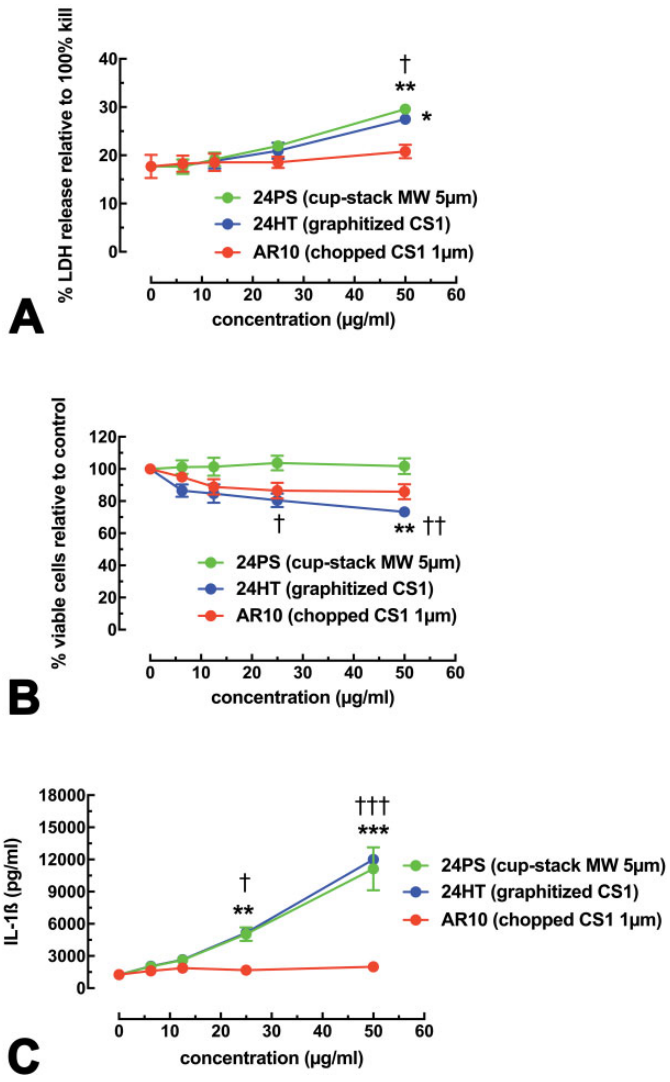

Figure 2. Cell viability data and IL-1β release for THP-1 cells exposed to the 3 multiwalled carbon nanotube (MWCNT) variants for 24 hr. Data expressed as mean ± SEM. (A) Cell viability by lactate dehydrogenase assay for the 3 MWCNT variants is shown. (B) Cell viability by 3-(4,5-dimethylthiazol-2-yl)-5-(3-carboxymethoxyphenyl)-2-(4-sulfophenyl)-2H-tetrazolium assay for the 3 MWCNT variants is shown. (C) IL-1β release for the 3 MWCNT variants is shown. Asterisks indicate significance *$p < .05$, **$p < .01$, and ***$p < .001$ compared to the 0 μg/ml no-particle control. Daggers indicate significance $^{\dagger}p < .05$, $^{\dagger\dagger}p < .01$, and $^{\dagger\dagger\dagger}p < .001$ compared to the AR10 MWCNT variant at the same concentration. Three experimental replicates were performed.

24HT MWCNT produced significant toxicity within 24 hr. The 24PS MWCNT showed no toxicity with this assay.

NLRP3 inflammasome activity was measured by proxy using IL-1β release as an end point in the 24-hr cultures. Figure 2C shows the IL-1β release data after stimulation by the 3 MWCNT variants. The 24PS and 24HT MWCNT produced significantly more IL-1β, in an essentially identical concentration-dependent manner, than that of both the no-particle control and AR10 at corresponding concentrations.

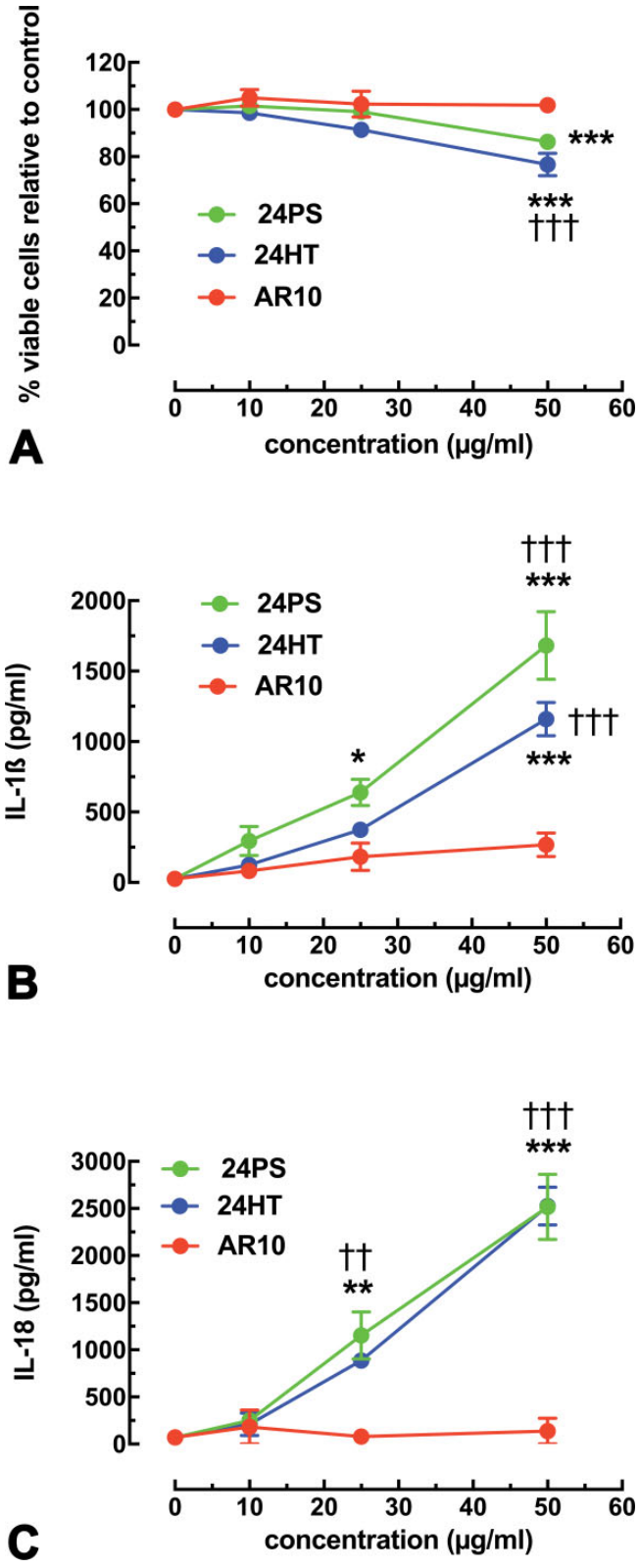

Figure 3. Cell viability data, IL-1β release, and IL-18 release for C57BL/6 alveolar macrophages exposed to the 3 multiwalled carbon nanotube (MWCNT) variants for 24 hr. Data expressed as mean ± SEM. (A) Cell viability by 3-(4,5-dimethylthiazol-2-yl)-5-(3-carboxymethoxyphenyl)-2-(4-sulfophenyl)-2H-tetrazolium assay for the 3 MWCNT variants is shown. (B) IL-1β release for the 3 MWCNT variants is shown. (C) IL-18 release for the 3 MWCNT variant is shown. Asterisks indicate significance *p < .05, **p < .01, and ***p < .001 compared to the 0 µg/ml no-particle control. Daggers indicate significance $^{\dagger}p$ < .05, $^{\dagger\dagger}p$ < .01, and $^{\dagger\dagger\dagger}p$ < .001 compared to the AR10 MWCNT variant at the same concentration. Three experimental replicates were performed.

These results clearly indicated that MWCNT length, and not surface reactivity, drives IL-1β release in response to the particle and was the preliminary basis for the other experiments. Furthermore, the THP-1 cell line appears to be a reliable model to evaluate particles (Hamilton, Wu, et al. 2013; Hamilton, Xiang, et al. 2013; Hamilton et al. 2014; Xia et al. 2013).

In Vitro *C57BL/6 AM Cytotoxicity and NLRP3 Inflammasome Activation*

The next *in vitro* model used AMs isolated from C57BL/6 mice exposed to the same 3 MWCNT variants. Figure 3A shows the toxicity of these nanomaterials in a 24-hr culture at various concentrations ranging from 6.25 µg/ml to 50 µg/ml. The MTS assay results demonstrate that both the original cup-stack 24PS and the heated 24HT MWCNT produced significantly more toxicity at the highest concentration tested than that of the 0 µg/ml control and the AR10 chopped MWCNT at the same concentration (50 µg/ml). Overall, these findings are similar to the THP-1 results.

Figure 3B and C shows the cytokine release related to NLRP3 inflammasome activation for AMs exposed to the 3 MWCNT variants. The 24PS and 24HT MWCNT produced significantly more IL-1β in a concentration-dependent manner than that of the no-particle control and the AR10 at corresponding concentrations (Figure 3B). Another NLRP3 inflammasome cytokine, IL-18, was assayed; the results were very similar to those observed for IL-1β. In this case, IL-18 was higher at both the 50 and 25 µg/ml concentrations for 24PS and 24HT MWCNT than that of the controls and short AR10 MWCNT at the same concentration. Image confirmation of *in vitro* cell death produced by the 24PS and 24HT MWCNT (25 µg/ml concentration for 24 hr) can be found in Figure 4. These findings are consistent with the THP-1 model results.

In Vivo *C57BL/6 Exposure and 24-hr Lavage Cell Count and Differential*

With the *in vitro* data clearly indicating that MWCNT length is the most important inflammatory factor, the 3 MWCNT variants were tested in an *in vivo* mouse exposure model as described in Methods section. One indicator of acute inflammation is an influx of polymorphonuclear (PMN) cells in the lungs of particle-exposed mice. Figure 5 shows PMN counts from the lungs 24 hr following MWCNT instillations. Figure 5A shows the data as a percentage of total cells retrieved in the lung lavage, and Figure 5B shows the absolute cell counts. Regardless of the way the data are presented, there were clearly

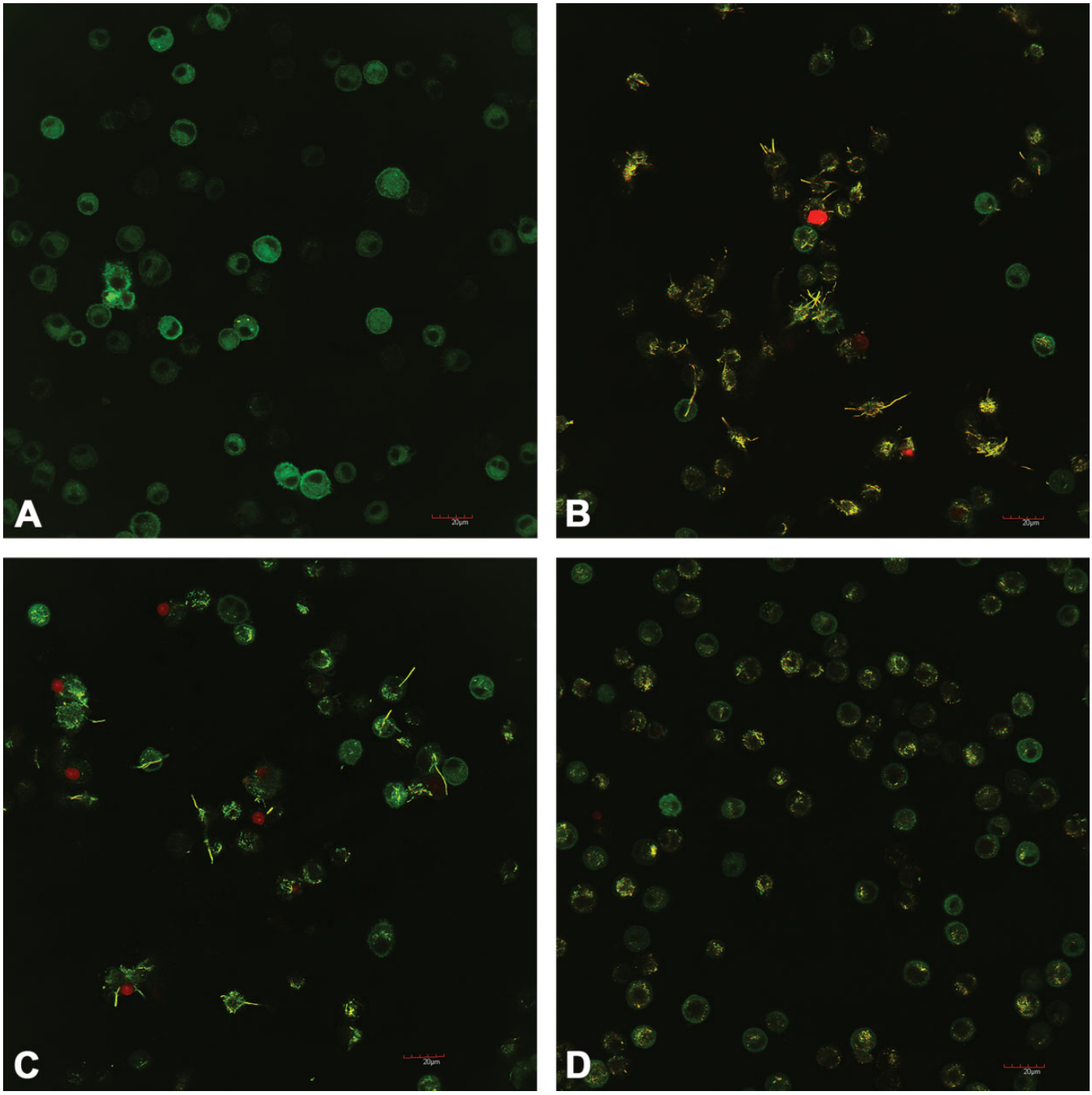

Figure 4. Representative confocal images of C57BL/6 (alveolar macrophage) exposed to multiwalled carbon nanotube (MWCNT) variants at 25 μg/ml for 24 hr. Cells were stained with a green membrane stain $DiOC_{18}(3)$ and a nucleic acid counterstain propidium iodide for 30 min in phosphate buffered saline prior to imaging at a 1,000× dilution as supplied in the LIVE/DEAD cell-mediated cytotoxicity kit (L7010) from molecular probes. Green cells indicated living cells. Red nuclei indicated dead cells. The yellow staining of the MWCNT resulted from the carbon absorbing the stains equally. (A) Dispersion media. (B) MWCNT 24PS at 25 μg/ml. (C) MWCNT 24HT at 25 μg/ml. (D) MWCNT AR10 at 25 μg/ml. The long yellow fibers in B (24PS) and C (24HT) can be easily distinguished from the short yellow fibers in D (AR10).

significant increases in PMN cells in the lung lavages from mice receiving the highest dose (40 μg) of 24PS and 24HT MWCNT, with the heat-treated 24HT producing the highest number of PMN cells. The short, chopped AR10 failed to create an inflammatory condition in the mouse lungs at any dose tested, consistent with the *in vitro* results above.

In addition to evaluating PMN cell inflammation, the concentrated lavage fluid was analyzed for indicators of acute

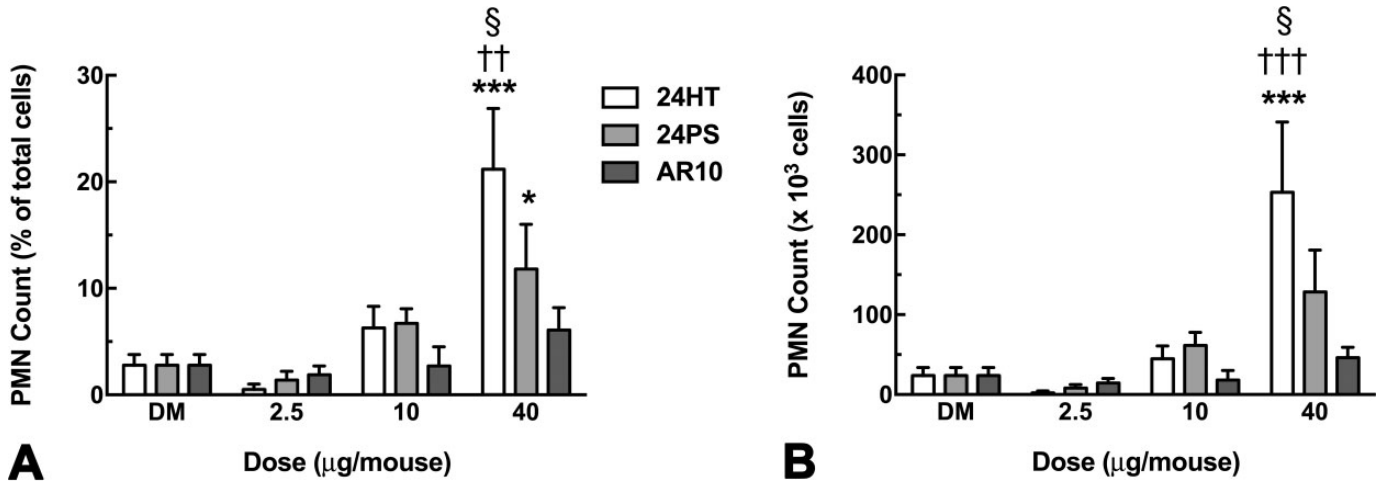

Figure 5. Polymorphonuclear (PMN) cell count from lung lavage 24-hr post multiwalled carbon nanotube (MWCNT) instillation. (A) Mean ± SEM PMN counts as percentage of total cells in lung lavage for all MWCNT instillation conditions are shown. (B) Mean ± SEM PMN counts as cell numbers for MWCNT instillation conditions are shown. Asterisks indicate significance $^{*}p < .05$ and $^{***}p < .001$ compared to dispersion media vehicle. Daggers indicate significance $^{††}p < .01$ and $^{†††}p < .001$ compared to the AR10 MWCNT variant at the same dose. Symbol indicates § at $p < .05$ compared to the 24PS MWCNT at the same dose. $n = 8$ mice per condition.

inflammation and lung injury at 24-hr postinstillation. Figure 6 shows the data for inflammasome-related cytokines (6A and 6B), cathepsin release (6C and 6D), HMGB1 (6E), and LDH (6F). IL-1β release did not achieve statistical significance; however, there was an increase in this cytokine at the highest dose (40 μg) for both 24PS and 24HT MWCNT instillations (Figure 6A). In contrast, there were significant increases in IL-18 for 24PS and 24HT-instilled mouse lungs at both the 10 and 40 μg doses. In these studies, IL-18 was a more sensitive indicator of NLRP3 inflammasome activation than IL1β. Total cathepsin (mixture of various cathepsins released from lysosomes) content of the lung lavage fluid (shown in Figure 6C) was significantly increased at the 10 μg concentration for the 24HT instillation only. However, cathepsin B activity increased significantly at the highest dose of the 24PS and 24HT MWCNT, but not AR10, instilled in the lungs, as shown in Figure 6D. HMGB1 release into lavage fluid, which has been implicated as an endogenous NF-κB stimulator (Jessop and Holian 2014), increased significantly in the lung lavage fluid from mice receiving 24HT MWCNT at the highest dose, whereas HMGB1 from mice receiving AR10 did not increase above baseline. Lastly, LDH, a marker of cell injury/death, was elevated in the lavage fluid from mice exposed to 24PS and 24HT at the highest dose (40 μg). Taken together, it was clear that heat-treated, graphitized MWCNT produced the same or a slightly higher inflammatory response than that of the original 24PS cup-stack MWCNT. In contrast, the chopped shortened AR10 MWCNT resulted in no detectible indications of acute inflammation in exposed mice; the AR10 material only differed from the bioactive 24PS by its length, which was approximately 5 times shorter or a fifth of the original length. These results support the hypothesis that length is an important MWCNT physical characteristic resulting in lung inflammation.

Human AM Exposure to MWCNT—Preliminary In Vitro *Result*

We were able to conduct a preliminary test with human AM to the MWCNT featured in this study. The human AM were cultured with and without 20 ng/ml LPS and with the MWCNT variants at 50 μg/ml. The resulting data are presented here as a preliminary result that correlates with the results presented in the models described above. The data are presented without statistical analysis, as the variability was caused from pseudoreplication (1 subject's cells used in more than 1 experimental replication) in 1 (1) experiment (Zar 2010). IL-1β production from human AM is shown in Figure 7. There was no IL-1β production in the absence of LPS, indicative of the need for NF-κB activation similar to observed for murine primary AM. However, in contrast to murine AM, the human AM costimulated with LPS showed a baseline release of IL-1β that increased with exposure to the 24PS and 24HT MWCNT variants. Results from cells exposed to the smaller AR10 MWCNT/LPS were the same as those from the control/LPS cells. This result was completely consistent with the results in the other models, indicating the importance of size and rigidity in stimulation of the NLRP3 inflammasome. Cell viability of MWCNT exposed cells compared to control cultures showed a slight decrease in viability with all MWCNT variants by MTS assay (~10%, *data not shown*).

Discussion

NLRP3 inflammasome activation clearly causes acute and chronic inflammation, resulting in lung pathologies (Sayan and Mossman 2016; Grailer et al. 2014; W. Yang et al. 2015; Aslan-Sungur et al. 2016). Understanding exactly how inhaled particles such as MWCNT trigger this cellular response is

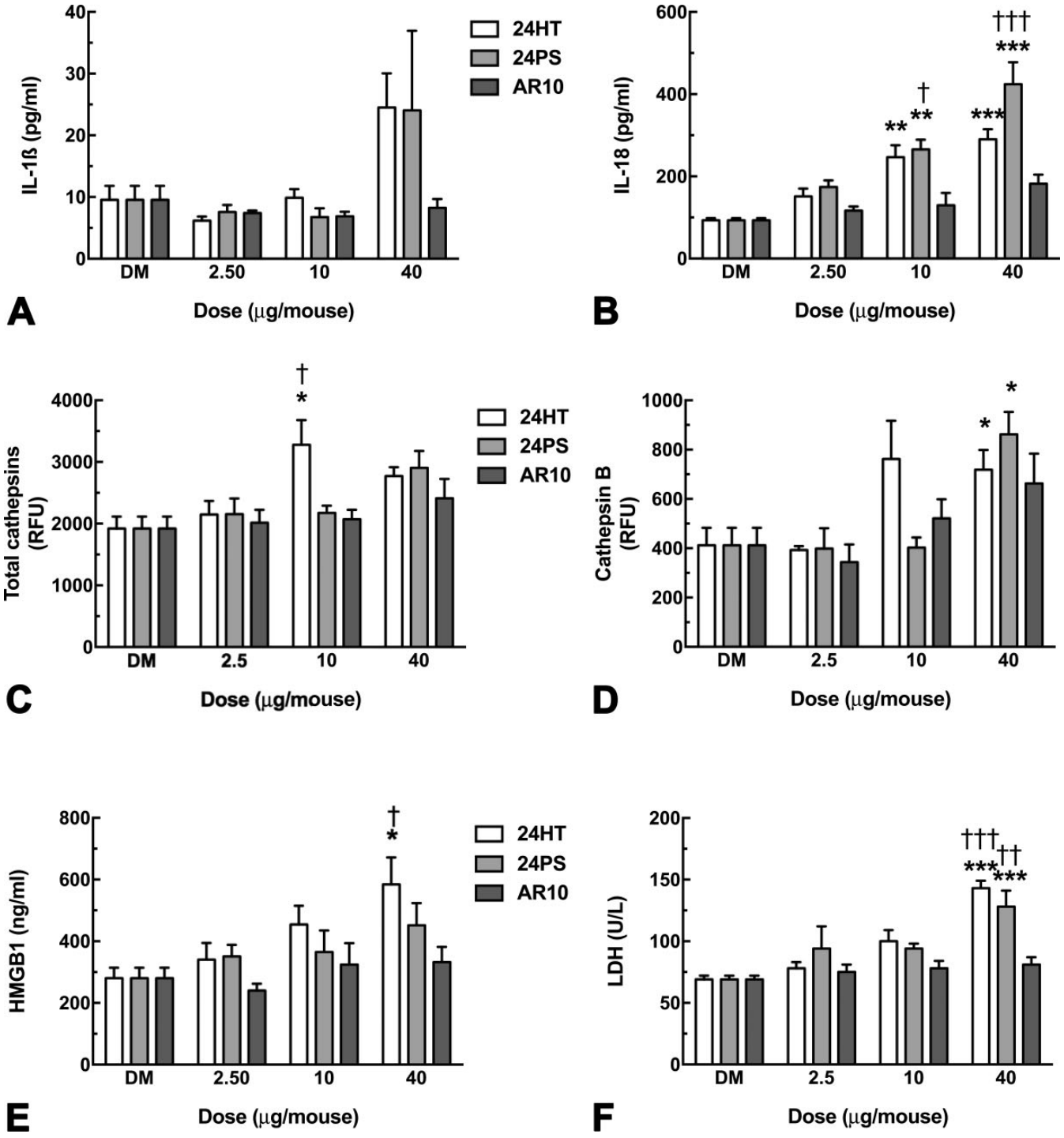

Figure 6. Summary data of lavage fluid markers of acute inflammation 24 hr following multiwalled carbon nanotube (MWCNT) instillations in the lungs of C57BL/6 mice. (A) Mean ± SEM IL-1β release is shown. (B) Mean ± SEM IL-18 release is shown. (C) Mean ± SEM total cathepsin release is shown. (D) Mean ± SEM cathepsin B release is shown. (E) Mean ± SEM HMGB1 release is shown. (F) Mean ± SEM lactate dehydrogenase release is shown. Asterisks indicate significance at $^{*}p < .05$, $^{**}p > .01$, or $^{***}p < .001$ compared to corresponding dispersion media vehicle. Daggers indicate significance at $^{\dagger}p < .05$, $^{\dagger\dagger}p < .01$, or $^{\dagger\dagger\dagger}p < .001$ compared to the AR19 MWCNT instillation condition at the same dose. $n = 8$ mice per condition.

important for developing effective therapeutics. Several studies, both *in vitro* and *in vivo*, have demonstrated that MWCNT with varying physical characteristics activate the NLRP3 inflammasome in macrophage cells, resulting in inflammation (Hamilton, Wu, et al. 2013; Hamilton, Xiang, et al. 2013). Because of the unique and valuable qualities of MWCNT,

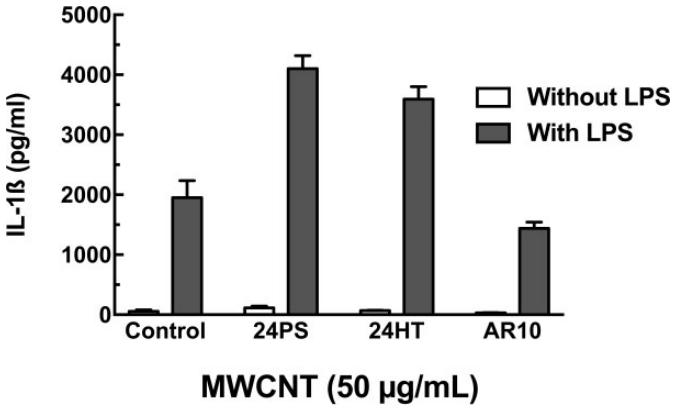

Figure 7. IL-1β production from human alveolar macrophages exposed to multiwalled carbon nanotube (MWCNT) with and without lipopolysaccharide (LPS). Means ± SEM IL-1β in 24-hr cultures with and without LPS are shown. MWCNT concentration was 50 µg/ml. No statistical evaluation was conducted, attributable to only 1 subject. Variance resulted from pseudoreplication.

human exposure is certain to increase over the next few years and beyond (Ono-Ogasawara and Myojo 2011; Hedmer et al. 2014; J. S. Lee et al. 2015). Therefore, elucidating exact mechanisms regarding how these particles initiate an inflammatory response is increasingly important.

Palomaki and colleagues (2011) demonstrated that rigid, long MWCNTs behave similar to asbestos fibers when taken up by macrophages. They concluded that both MWCNT and asbestos fibers activate the NLRP3 inflammasome through a mechanism involving ROS production. Further, Palomaki et al. established the concept that length, aspect ratio, and particle rigidity are important characteristics regarding NLRP3 inflammasome activation; ROS are cited as the mechanism of action, similar to results reported in an earlier paper on asbestos (Dostert et al. 2008). The role of ROS has been cited more recently as playing an important role in MWCNT-induced genotoxicity in mouse fibroblast cells (Alarifi and Ali 2015). Another recent study demonstrated CNT-associated declines in lung epithelial cell proliferation that correlated with ROS generating capacity and high surface area of the particles (Jackson et al. 2015). Other studies have pointed to ROS generation as a primary adverse effect of MWCNT by demonstrating reduced antioxidant capacity following exposure in marine organisms (J. W. Lee et al. 2016), and suppression of MWCNT-induced lung fibrosis in wild-type animals administered N-acetyl-cysteine (Sun et al. 2015). Further, MWCNT-induced bacterial cell death has been attributed to damage to the bacterial cell membrane by ROS (Rajavel et al. 2014)

While the presence of ROS following MWCNT exposure and their contribution to cellular damage is undeniable, the exact role they play in initiating MWCNT-induced pathologies has not been definitively confirmed. Unfortunately, most ROS/inflammasome-related research uses nigericin to stimulate cells (Heid et al. 2013; Nomura et al. 2015; Antonopoulos et al. 2015; Guey et al. 2014; Yaron et al. 2016). Nigericin acts as a H^+, K^+ ionophore (Bissinger et al. 2016) and antiporter of H^+ and K^+ ions (Bissinger et al. 2016; Budunova and Mittelman 1992). This is important for 3 reasons. First, nigericin is not a particle and is, therefore, not processed as a particle by the cell; particles are taken into a phagosome fused to a lysosome. Second, K^+ efflux has been shown to be important for NLRP3 inflammasome activation (Katsnelson et al. 2015), and nigericin directly affects this function (Katsnelson et al. 2015). Finally, nigericin affects pH stability in cells (Bevensee, Bashi, and Boron 1999). These observations negate the use of nigericin as a representative model for particle-induced NLRP3 inflammasome activation or LMP. As such, the results of this study suggest that any ROS are a consequence of MWCNT-induced LMP rather than a contributor to the key step of LMP.

Consistent with Palomaki, several studies have implicated particle size (length and diameter) in MWCNT-induced NLRP3 inflammasome activation and subsequent inflammation (Hamilton, Wu, et al. 2013; Murphy et al. 2013). This is not unique to MWCNT exposure, however, as it occurs with other bioactive nanomaterials (Hamilton et al. 2009; Hamilton, Buckingham, and Holian 2014; Ji et al. 2012; Poland et al. 2012; Kusaka et al. 2014). The current study used cup-stack MWCNT of 2 different lengths without affecting ROS potential (either generation or elimination; Tsuruoka, Matsumoto, Castranova, et al. 2015;Tsuruoka, Matsumoto, Koyama, et al. 2015). It is important to note that if surface reactivity of the 24PS was essential to its bioactivity, then the AR10 material should have been more potent since it had a higher surface area for the same mass as 24PS. In contrast, 24HT had its surface graphitized, yet had the same bioactivity as the original cup-stack 24PS MWCNT. Table 1 illustrates ROS potential in the category "electrical resistance in a bulk state." Values for the short (AR10) and long (24PS) MWCNT are very similar, whereas the value for heat-treated (24HT) MWCNT is negligible. These data validate the experimental manipulation of test particles used throughout the study. All data are consistent, indicating that short (AR10) MWCNTs are more inert than that of the other 2 MWCNTs, implying that length or size is more important than surface properties with regard to MWCNT particle-induced toxicity, NLRP3 inflammasome activation, and/or acute inflammation. These data contradict the hypothesis that nanomaterial activation of the NLRP3 inflammasome is dependent upon ROS potential. Further, these data support the notion that ROS result from MWCNT-induced LMP causing mitochondrial dysfunction. In the current studies, we did not present evidence to evaluate whether mitochondrial dysfunction leads to or follows ROS generation. The current proposed mechanism of nanoparticle-induced acute inflammation through macrophages initiates with LMP and release of cathepsin B. Since cathepsin B was released as shown by our data (Figure 5D), we hypothesize that other lysosomal proteolytic enzymes were released that would be capable of causing mitochondrial injury (Bunderson-Schelvan et al. 2016). Nevertheless, the mechanism responsible for induction of lysosomal membrane instability is not clear. In order to address

this gap of knowledge, we are activity pursuing the mechanism(s) to explain how bioactive nanoparticles alter the movement of membrane lipids leading to pore formation in phagolysosomes leading to enzymatic release.

Accurate measurement and source of ROS is challenging with living cells, as the source and reaction kinetics are complicated. On the other hand, it is possible to estimate redox potential in the present study. The scavenger rate of the radicals in MWCNT aqueous solutions have been reported (Tsuruoka et al. 2013). As described, the scavenger rate per unit MWCNT weight corresponds to the surface morphology (see Figure 4 in the cited report). Surface electrical resistance is one of the typical properties used for this metric. For that reason, resistance is being used in the present study. The redox potential depends on the MWCNT concentration in addition to other chemical species. Therefore, the electrical resistance most accurately indicates the relative ROS potential in the present experimental conditions.

In conclusion, we suggest that the results of this study are consistent with LMP being a key regulator in nanoparticle toxicity and lung inflammation. Although ROS are generated during nanoparticle toxicity and contribute to cell injury, they do not appear responsible for LMP. Further, the results of this study have important implications for the research design of future studies and will hopefully stimulate a reexamination of the results from previous studies. Going forward, well-designed studies should yield an improved understanding of the various underlying processes associated with particle toxicity.

Authors' Note

The findings and conclusions in this report are those of the authors and do not necessarily represent the views of the National Institute for Occupational Safety and Health.

Author Contribution

Authors contributed to conception or design (RH, ST, NW, DP, AH); data acquisition, analysis, or interpretation (RH, ST, MW, DP, MB, AH); drafting the manuscript (RH); and critically revising the manuscript (RH, ST, NW, MW, DP, MB, AH). All authors gave final approval and agreed to be accountable for all aspects of work in ensuring that questions relating to the accuracy or integrity of any part of the work are appropriately investigated and resolved.

Declaration of Conflicting Interests

The author(s) declared no potential conflicts of interest with respect to the research, authorship, and/or publication of this article.

Funding

The author(s) disclosed receipt of the following financial support for the research, authorship, and/or publication of this article: Shuji Tsuruoka was supported by the Center of Innovation Program, "Global Aqua Innovation Center for Improving Living Standards and Water-sustainability" from Japan Science and Technology Agency, JST.

References

Alarifi, S, and Ali, D. (2015). Mechanisms of multi-walled carbon nanotubes-induced oxidative stress and genotoxicity in mouse fibroblast cells. *Int J Toxicol* **34**, 258–265.

Antonopoulos, C., Russo, H. M., El Sanadi, C., Martin, B. N., Li, X., Kaiser, W. J., Mocarski, E. S., and Dubyak, G. R. (2015). Caspase-8 as an effector and regulator of NLRP3 inflammasome signaling. *J Biol Chem* **290**, 20167–84.

Arend, W. P., Palmer, G., and Gabay, C. (2008). IL-1, IL-18, and IL-33 families of cytokines. *Immunol Rev* **223**, 20–38.

Aslan-Sungur, G., Lee, X., Evrendilek, F., and Karakaya, N. (2016). Large interannual variability in net ecosystem carbon dioxide exchange of a disturbed temperate peatland. *Sci Total Environ* **554**, 192–202.

Bevensee, M. O., Bashi, E., and Boron, W. F. (1999). Effect of trace levels of nigericin on intracellular pH and acid-base transport in rat renal mesangial cells. *J Membr Biol* **169**, 131–39.

Bissinger, R., Malik, A., Bouguerra, G., Zhou, Y., Singh, Y., Abbes, S., and Lang, F. (2016). Triggering of suicidal erythrocyte death by the antibiotic ionophore nigericin. *Basic Clin Pharmacol Toxicol* **118**, 381–89.

Budunova, I. V., and Mittelman, L. A. (1992). The effect of K+/H+ antiporter nigericin on gap junction permeability. *Cell Biol Toxicol* **8**, 63–73.

Bunderson-Schelvan, M., Hamilton, R., Trout, K., Jessop, F., Gulumian, M., and Holian, A. (2016). Approaching a unified theory for particle-induced inflammation. In *Biological Effects of Fibrous and Particulate Substances* (T. Otsuki, Y. Yasuo, and A. Holian eds.), pp. 51–76. Springer, Wako, Japan.

Donaldson, K., Aitken, R., Tran, L., Stone, V., Duffin, R., Forrest, G., and Alexander, A. (2006). Carbon nanotubes: a review of their properties in relation to pulmonary toxicology and workplace safety. *Toxicol Sci* **92**, 5–22.

Donaldson, K., Murphy, F. A., Duffin, R., and Poland, C. A. (2010). Asbestos, carbon nanotubes and the pleural mesothelium: a review of the hypothesis regarding the role of long fibre retention in the parietal pleura, inflammation and mesothelioma. *Part Fibre Toxicol* **7**, 5.

Dostert, C., Petrilli, V., Van Bruggen, R., Steele, C., Mossman, B. T., and Tschopp, J. (2008). Innate immune activation through Nalp3 inflammasome sensing of asbestos and silica. *Science* **320**, 674–77.

Fenoglio, I., Aldieri, E., Gazzano, E., Cesano, F., Colonna, M., Scarano, D., Mazzucco, G., et al. (2012). Thickness of multiwalled carbon nanotubes affects their lung toxicity. *Chem Res Toxicol* **25**, 74–82.

Grailer, J. J., Canning, B. A., Kalbitz, M., Haggadone, M. D., Dhond, R. M., Andjelkovic, A. V., Zetoune, F. S., and Ward, P. A. (2014). Critical role for the NLRP3 inflammasome during acute lung injury. *J Immunol* **192**, 5974–83.

Guey, B., Bodnar, M., Manie, S. N., Tardivel, A., and Petrilli, V. (2014). Caspase-1 autoproteolysis is differentially required for NLRP1b and NLRP3 inflammasome function. *Proc Natl Acad Sci U S A* **111**, 17254–59.

Hamilton, R. F., Buckingham, S., and Holian, A. (2014). The effect of size on Ag nanosphere toxicity in macrophage cell models and lung epithelial cell lines is dependent on particle dissolution. *Int J Mol Sci* **15**, 6815–30.

Hamilton, R. F., Girtsman, T. A., Xiang, C., Wu, N., and Holian, A. (2013). Nickel contamination on MWCNT is related to particle bioactivity but not toxicity in the THP-1 transformed macrophage model. *Int J Biomed Nanosci Nanotechnol* **3**, 107–126.

Hamilton, R. F., Wu, N., Porter, D., Buford, M., Wolfarth, M., and Holian, A. (2009). Particle length-dependent titanium dioxide nanomaterials toxicity and bioactivity. *Part Fibre Toxicol* **6**, 35.

Hamilton, R. F., Wu, N., Xiang, C., Li, M., Yang, F., Wolfarth, M., Porter, D. W., and Holian, A. (2014). Synthesis, characterization, and bioactivity of carboxylic acid-functionalized titanium dioxide nanobelts. *Part Fibre Toxicol* **11**, 43.

Hamilton, R. F., Wu, Z., Mitra, S., Shaw, P. K., and Holian, A. (2013). Effect of MWCNT size, carboxylation, and purification on in vitro and in vivo toxicity, inflammation and lung pathology. *Part Fibre Toxicol* **10**, 57–74.

Hamilton, R. F. Jr., Buford, M., Xiang, C., Wu, N., and Holian, A. (2012). NLRP3 inflammasome activation in murine alveolar macrophages and related lung pathology is associated with MWCNT nickel contamination. *Inhal Toxicol* **24**, 995–1008.

Hamilton, R. F. Jr., Xiang, C., Li, M., Ka, I., Yang, F., Ma, D., Porter, D. W., Wu, N., and Holian, A. (2013). Purification and sidewall functionalization of multiwalled carbon nanotubes and resulting bioactivity in two macrophage models. *Inhal Toxicol* **25**, 199–210.

Hedmer, M., Isaxon, C., Nilsson, P. T., Ludvigsson, L., Messing, M. E., Genberg, J., Skaug, V., et al. (2014). Exposure and emission measurements during production, purification, and functionalization of arc-discharge-produced multi-walled carbon nanotubes. *Ann Occup Hyg* **58**, 355–79.

Heid, M. E., Keyel, P. A., Kamga, C., Shiva, S., Watkins, S. C., and Salter, R. D. (2013). Mitochondrial reactive oxygen species induces NLRP3-dependent lysosomal damage and inflammasome activation. *J Immunol* **191**, 5230–38.

Jackson, P., Kling, K., Jensen, K. A., Clausen, P. A., Madsen, A. M., Wallin, H., and Vogel, U. (2015). Characterization of genotoxic response to 15 multiwalled carbon nanotubes with variable physicochemical properties including surface functionalizations in the FE1-Muta(TM) mouse lung epithelial cell line. *Environ Mol Mutagen* **56**, 183–203.

Jessop, F., and Holian, A. (2015). Extracellular HMGB1 regulates multi-walled carbon nanotube-induced inflammation in vivo. *Nanotoxicology* **9**, 365–372.

Ji, Z., Wang, X., Zhang, H., Lin, S., Meng, H., Sun, B., George, S., et al. (2012). Designed synthesis of CeO2 nanorods and nanowires for studying toxicological effects of high aspect ratio nanomaterials. *ACS Nano* **6**, 5366–80.

Katsnelson, M. A., Rucker, L. G., Russo, H. M., and Dubyak, G. R. (2015). K+ efflux agonists induce NLRP3 inflammasome activation independently of Ca2+ signaling. *J Immunol* **194**, 3937–52.

Kusaka, T., Nakayama, M., Nakamura, K., Ishimiya, M., Furusawa, E., and Ogasawara, K. (2014). Effect of silica particle size on macrophage inflammatory responses. *PLoS One* **9**, e92634.

Lee, J. S., Choi, Y. C., Shin, J. H., Lee, J. H., Lee, Y., Park, S. Y., Baek, J. E., et al. (2015). Health surveillance study of workers who manufacture multi-walled carbon nanotubes. *Nanotoxicology* **9**, 802–11.

Lee, J. W., Won, E. J., Kang, H. M., Hwang, D. S., Kim, D. H., Kim, R. K., Lee, S. J., and Lee, J. S. (2016). Effects of multi-walled carbon nanotube (MWCNT) on antioxidant depletion, the ERK signaling pathway, and copper bioavailability in the copepod (*Tigriopus japonicus*). *Aquat Toxicol* **171**, 9–19.

Lehman, J. H., Terrones, M., Mansfield, E., Hurst, K. E., and Meunier, V. (2011). Evaluating the characteristics of multiwall carbon nanotubes. *Carbon* **49**, 2581–602.

Liu, X., Guo, L., Morris, D., Kane, A. B., and Hurt, R. H. (2008). Targeted removal of bioavailable metal as a detoxification strategy for carbon nanotubes. *Carbon N Y* **46**, 489–500.

Martinon, F., Mayor, A., and Tschopp, J. (2009). The inflammasomes: guardians of the body. *Annu Rev Immunol* **27**, 229–65.

Menendez, J. A., Phillips, J., Xia, B., and Radovic, L. R. (1996). On the modification and characterization of chemical surface properties of activated carbon: in the search of carbons with stable basic properties. *Langmuir* **12**, 4404–10.

Mercer, R. R., Hubbs, A. F., Scabilloni, J. F., Wang, L., Battelli, L. A., Schwegler-Berry, D., Castranova, V., and Porter, D. W. (2010). Distribution and persistence of pleural penetrations by multi-walled carbon nanotubes. *Part Fibre Toxicol* **7**, 28.

Murphy, F. A., Poland, C. A., Duffin, R., Al-Jamal, K. T., Ali-Boucetta, H., Nunes, A., Byrne, F., et al. (2011). Length-dependent retention of carbon nanotubes in the pleural space of mice initiates sustained inflammation and progressive fibrosis on the parietal pleura. *Am J Pathol* **178**, 2587–600.

Murphy, F. A., Poland, C. A., Duffin, R., and Donaldson, K. (2013). Length-dependent pleural inflammation and parietal pleural responses after deposition of carbon nanotubes in the pulmonary airspaces of mice. *Nanotoxicology* **7**, 1157–67.

Nel, A., Xia, T., Madler, L., and Li, N. (2006). Toxic potential of materials at the nanolevel. *Science* **311**, 622–27.

Nomura, J., So, A., Tamura, M., and Busso, N. (2015). Intracellular ATP decrease mediates NLRP3 inflammasome activation upon nigericin and crystal stimulation. *J Immunol* **195**, 5718–24.

Ono-Ogasawara, M., and Myojo, T. (2011). A proposal of method for evaluating airborne MWCNT concentration. *Ind Health* **49**, 726–34.

Palomaki, J., Valimaki, E., Sund, J., Vippola, M., Clausen, P. A., Jensen, K. A., Savolainen, K., Matikainen, S., and Alenius, H. (2011). Long, needle-like carbon nanotubes and asbestos activate the NLRP3 inflammasome through a similar mechanism. *ACS Nano* **5**, 6861–70.

Poland, C. A., Byrne, F., Cho, W. S., Prina-Mello, A., Murphy, F. A., Davies, G. L., Coey, J. M., et al. (2012). Length-dependent pathogenic effects of nickel nanowires in the lungs and the peritoneal cavity. *Nanotoxicology* **6**, 899–911.

Porter, D., Sriram, K., Wolfarth, M., Jefferson, A., Schwegler-Berry, D., Andrew, M., and Castranova, V. (2008). A biocompatible medium for nanoparticle dispersion. *Nanotoxicology* **2**, 144–54.

Porter, D. W., Hubbs, A., Chen, B. T., McKinney, W., Mercer, R., Wolfarth, M., Battelli, L., et al. (2013). Acute pulmonary dose-responses to inhaled multi-walled carbon nanotubes. *Nanotoxicology* **7**, 1179–1194.

Porter, D. W., Hubbs, A. F., Mercer, R. R., Wu, N., Wolfarth, M. G., Sriram, K., Leonard, S., et al. (2010). Mouse pulmonary dose- and time course-responses induced by exposure to multi-walled carbon nanotubes. *Toxicology* **269**, 136–47.

Qu, G. B., Bai, Y. H., Zhang, Y., Jia, Q., Zhang, W. D., and Yan, B. (2009). The effect of multiwalled carbon nanotube agglomeration on their accumulation in and damage to organs in mice. *Carbon N Y* **47**, 2060–69.

Rajavel, K., Gomathi, R., Manian, S., and Rajendra Kumar, R. T. (2014). In vitro bacterial cytotoxicity of CNTs: reactive oxygen species mediate cell damage edges over direct physical puncturing. *Langmuir* **30**, 592–601.

Sager, T. M., Wolfarth, M. W., Andrew, M., Hubbs, A., Friend, S., Chen, T. H., Porter, D. W., et al. (2014). Effect of multi-walled carbon nanotube surface modification on bioactivity in the C57BL/6 mouse model. *Nanotoxicology* **8**, 317–27.

Sayan, M., and Mossman, B. T. (2016). The NLRP3 inflammasome in pathogenic particle and fibre-associated lung inflammation and diseases. *Part Fibre Toxicol* **13**, 51.

Sun, B., Wang, X., Ji, Z., Wang, M., Liao, Y. P., Chang, C. H., Li, R., et al. (2015). NADPH oxidase-dependent NLRP3 inflammasome activation and its important role in lung fibrosis by multiwalled carbon nanotubes. *Small* **11**, 2087–97.

Tschopp, J., and Schroder, K. (2010). NLRP3 inflammasome activation: the convergence of multiple signalling pathways on ROS production? *Nat Rev Immunol* **10**, 210–15.

Tsuruoka, S., Matsumoto, H., Castranova, V., Porter, D. W., Yanagisawa, T., Saito, N., Kobayashi, S., and Endo, M. (2015). Differentiation of chemical reaction activity of various carbon nanotubes using redox potential: classification by physical and chemical structures. *Carbon N Y* **95**, 302–8.

Tsuruoka, S., Matsumoto, H., Koyama, K., Akiba, E., Yanagisawa, T., Cassee, F. R., Saito, N., et al. (2015). Radical scavenging reaction kinetics with multiwalled carbon nanotubes. *Carbon N Y* **83**, 232–39.

Tsuruoka, S., Takeuchi, K., Koyama, K., Noguchi, T., Endo, M., Tristan, F., Terrones, M., et al. (2013). ROS evaluation for a series of CNTs and their derivatives using an ESR method with DMPO. *J Phys Conf Ser* **429**, 012029.

Wang, X., Xia, T., Ntim, S. A., Ji, Z., Lin, S., Meng, H., Chung, C. H., et al. (2011). Dispersal state of multiwalled carbon nanotubes elicits profibrogenic cellular responses that correlate with fibrogenesis biomarkers and fibrosis in the murine lung. *ACS Nano* **5**, 9772–87.

Xia, T., Hamilton, R. F., Bonner, J. C., Crandall, E. D., Elder, A., Fazlollahi, F., Girtsman, T. A., et al. (2013). Interlaboratory evaluation of in vitro cytotoxicity and inflammatory responses to engineered nanomaterials: the NIEHS nano GO consortium. *Environ Health Perspect* **121**, 683–90.

Yang, M., Zhang, M., Tahara, Y., Chechetka, S., Miyako, E., Iijima, S., and Yudasaka, M. (2014). Lysosomal membrane permeabilization: carbon nanohorn-induced reactive oxygen species generation and toxicity by this neglected mechanism. *Toxicol Appl Pharmacol* **280**, 117–26.

Yang, W., Ni, H., Wang, H., and Gu, H. (2015). NLRP3 inflammasome is essential for the development of chronic obstructive pulmonary disease. *Int J Clin Exp Pathol* **8**, 13209–16.

Yaron, J. R., Rao, M. Y., Gangaraju, S., Zhang, L., Kong, X., Su, F., Tian, Y., Glenn, H. L., and Meldrum, D. R. (2016). The oxindole Syk inhibitor OXSI-2 blocks nigericin-induced inflammasome signaling and pyroptosis independent of potassium efflux. *Biochem Biophys Res Commun* **472**, 545–50.

Zar, J. H. (2010). *Biostatistical Analysis*. Pearson, Upper Saddle River, NJ.